OPEN ACCESS

**Saudi Journal of Engineering and Technology**
Abbreviated Key Title: Saudi J Eng Technol
ISSN 2415-6272 (Print) |ISSN 2415-6264 (Online)
Scholars Middle East Publishers, Dubai, United Arab Emirates
Journal homepage: https://saudijournals.com

**Original Research Article**

# Shielding Offshore Gas Turbines: A Validated CFD Approach to Multistage Inlet-Air Filtration

Samuel O. Effiom[1]*, Fidelis I. Abam[2], Assam T. Assam[1], Precious-Chibuzo O. Effiom[3], Okwonna C. Onochie[4], Oliver I. Inah[1]

[1]Department of Mechanical Engineering, Faculty of Engineering, University of Cross River State, Calabar, Nigeria
[2]Department of Mechanical Engineering, Faculty of Engineering & Technology, University of Calabar, Calabar, Nigeria
[3]Department of Petroleum Engineering, Faculty of Engineering & Technology, University of Calabar, Calabar, Nigeria
[4]Department of Mechanical Engineering, Abia State University, Uturu, Nigeria

**DOI:** https://doi.org/10.36348/sjet.2026.v11i01.003 | **Received:** 24.11.2025 | **Accepted:** 16.01.2026 | **Published:** 19.01.2026

***Corresponding author:** Samuel O. Effiom
Department of Mechanical Engineering, Faculty of Engineering, University of Cross River State, Calabar, Nigeria

## Abstract

Gas turbines (GTs) operating in offshore environments are highly vulnerable to performance degradation from airborne contaminants such as salt aerosols, mist, hydrocarbons, and particulate matter. This study develops and validates a computational fluid dynamics (CFD) model to optimize a multistage inlet-air filtration system for offshore GT applications, complementing prior experimental investigations. A three-dimensional CAD model of a wind tunnel housing six ASHRAE filter classes (F7, H12, E11, E10, G5, F9) was created in ANSYS Design Modeler, and simulations were performed under steady-state and transient conditions using Navier–Stokes, turbulence, and particle transport models. Contaminant mass loadings from 20–100% were evaluated at inlet velocities of 5 m/s and 10 m/s to characterize airflow distribution, static and total pressures, and filtration efficiency. Results revealed peak inlet velocities up to nine times the free-stream value, with mass flow concentration opposite the vertical inflow reaching 8.4 kg/s. Static and total pressures decreased progressively downstream, with the highest pressure drops occurring at 80% contaminant loading, indicating increased flow resistance. Transient analyses showed filtration efficiency degradation over time due to fouling. Model predictions for total pressure drop and volumetric flow rate deviated by ≤10% from experimental data, confirming robustness and accuracy. This work offers validated CFD insights into the complex aero–particle dynamics in offshore GT inlet filtration, providing a predictive framework for optimizing filter design, selection, and maintenance to enhance long-term turbine reliability and efficiency.

**Keywords:** Computational fluid dynamics; gas turbine; inlet filtration; offshore environment; particle fouling; multistage filters.



## 1. INTRODUCTION

Gas turbines (GTs) for offshore applications are the main power drivers for oil exploration and production facilities [1, 2]. GTs are predominantly large consumers of ambient air and the volume and quality of ingested air is paramount for efficient operation, better output, and longevity of the GTs [3]. However, GTs operated offshore are susceptible to harsh environmental contaminants including; corrosive elements from aerosols, fog, mist, saltwater, particulate matter, hydrocarbons, and other pollutants present in the offshore environment [4, 5]. This can lead to increased wear and damage to compressor blades (compressor fouling and Erosion), resulting in decreased efficiency and elevated maintenance costs [6, 7]. To ameliorate these challenges, the development and optimization of inlet filtration systems have become a focal point of research in an effort to safeguard the turbine components and ensure optimal performance [7, 8].

The implementation of multistage inlet filtration systems is a recognized strategy to enhance the performance of gas turbines in offshore environments [9, 10]. These systems are designed to filter contaminants from the ingested air depending on the prevalent contaminants, selected filters, filter

combination/arrangements, GT usage, and health monitoring [4, 10, 11]. However, studies have shown that the complex flow patterns, variable particle concentrations, and dynamic conditions in offshore environments make the design configuration and optimization of these filtration systems challenging [12, 13]. To address this, researches have been ongoing in the last few decades using prognostics approaches categorized as experimental and numerical.

Howes [14], examined the criteria for selecting gas turbine inlet air systems, focusing on retrofit applications. However, the study provided limited insight into offshore conditions, which involve harsher contaminants in challenging operational environments. Brekke [15] addressed the gap between standardized tests and actual operational conditions in offshore gas turbine air filtration. This study emphasized that the test standards may not fully replicate the hostile conditions experienced offshore, thereby affecting the assessment of the filter performance. [16] conducted a performance evaluation of air filters through design optimization, presenting a framework that highlights the importance of filter efficiency in enhancing the quality of ingested air. However, this approach did not specifically address variations in contaminant types and sizes typically encountered in offshore environments. [17] investigated the impact of air filter design on heavy-duty diesel engines at different altitudes through experimental and numerical methods. Their findings highlighted the significance of filter configuration in reducing particulate load, though the focus on diesel engines limits its direct application to gas turbines.[18] modelled an air filter for automobile engines, exploring the impacts of filter design on intake efficiency. The study laid emphasis on automotive applications with limitation on specific research regarding gas turbine applications, especially in offshore environments. [19] assessed the impact of inlet filter pressure loss on single and two-spool gas turbines, highlighting the role of filtration on the gas turbines' performance. This study provided insight into pressure losses due to filters, though it did not explore specific offshore conditions. [20] carried out a 3D numerical modeling to evaluate flow patterns and pressure loss in gas turbine air intake systems, particularly in V94.2.5 turbines. Their findings demonstrated how intake design affects pressure loss, although practical offshore environments were not part of the study. [21] carried out another investigation on filtration systems in relation to particle fouling in gas turbine compressors. Their research suggested that uncaptured particles could cause significant fouling issues, stressing the need for efficient filtration systems. However, the study did not focus on offshore contaminants. [22] investigated the flow and pressure patterns across a filter housing. The study considered a 3-stage filtration system incorporated in a filter housing for a specific offshore environment. However, this approach lacked adequate experimental data from literature for proper result validation.[23] carried out a comparative CFD evaluation of 2D and 3D models of gas turbine filter houses, emphasizing that 3D models provided more accurate simulations of airflow and pressure patterns. However, the research did not consider filtration performance under offshore contaminant loads. Furthermore, [24] developed models to predict clogging in filters within heavy-duty gas turbine power systems, though experimental validation under offshore-specific contaminants would enhance its applicability. [25] examined the influence of oil content on particle loading in a two-stage filtration system, concluding that oil presence significantly affects filtration efficiency. This study is relevant to offshore environments, where oil aerosols are prevalent, though further exploration into different contaminant types would strengthen its findings. [10] further carried out an experimental study using real-time data of a typical offshore GT filtration test rig. In this study, several ASHRAE filter grades, filter configurations, and offshore contaminants of varied sizes were investigated in a wind tunnel, to obtain a suitable inlet filtration system for the studied offshore environment. This study was not numerically validated with recent literatures that have similar operating conditions.

This and other findings as recorded in the literatures have birthed the novelty of the current work. Therefore, the current study focuses on the development of a CFD model to evaluate the filtration system of an offshore oilfield GT with similar operating conditions. It also aims at validating the experimental model and results of [10] that established the optimal filtration system suitable for a specified offshore environment. The study also seeks to provide valuable insights that can assist GT manufacturers and users in the design, selection, maintenance, and replacement of inlet filtration systems, to enhance the efficiency and reliability of gas turbines in offshore environments.

## 2. METHODOLOGY

Figure 1 shows a flowchart describing the process of developing the CFD solution of the inlet air filtration model.

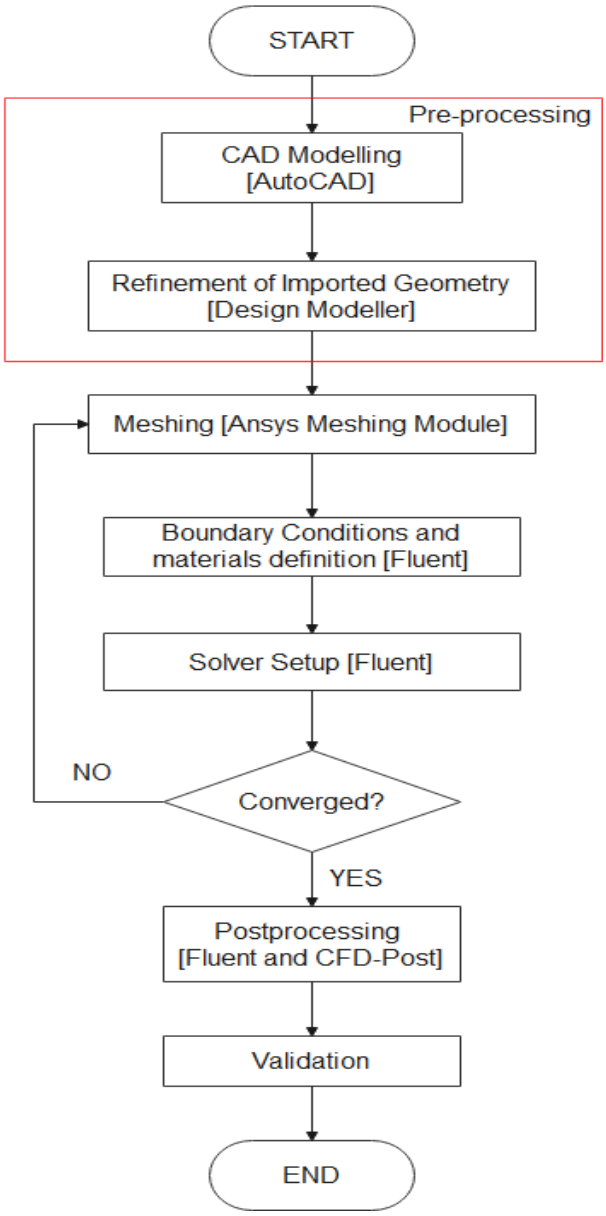


**Figure 1: Flowchart for the CFD analysis of the inlet air filter**

CAD model was developed and the geometry refined by the ANSYS design modeller for a wind tunnel configured with six classes of ASHRAE F7, H12, E11, E10, G5, and F9 filter elements. These filter elements conform to Filter A, B, C, D, E, and F respectively. The specified filter data is presented in Table 1. During the geometry refinement, irrelevant features were removed, such as the suction blower, the support frame of the wind tunnel, and other parts of the experimental setup, that were not required for the ANSYS fluent CFD simulation. Also, the computational domain was developed (See Figure 2). Meshing was further done (see Figure 3), and the materials, boundary conditions, and solver parameter were defined.

**Table 1: Filter data**

| Filter Elements | Average filtration efficiency (%) | Nominal air volume ($m^3/h$) | Initial pressure drop (Pa) | Final pressure drop (Pa) |
|---|---|---|---|---|
| F7 | > 90% (at 0.4$\mu m$) | 3400 | 100 | 450 |
| H12 | > 99.5% (at 0.5$\mu m$) | – | – | – |
| E11 | > 95% (at MPPS) | – | 140 | 400 |
| E10 | ≥ 85% | – | 130 | 400 |
| G5 | > 95% (at MPPS) | – | – | – |
| F9 | ≥ 95% (at 0.4$\mu m$) | 850 | 70 | 450 |

***MPPS**: Maximum power point speed*

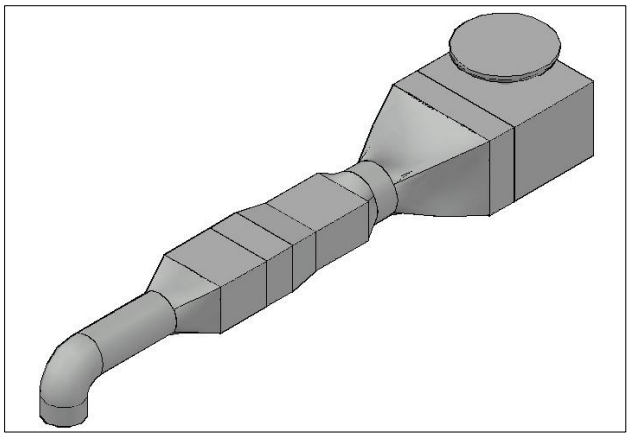

**Figure 2: Computational domain developed in ANSYS design modeller**

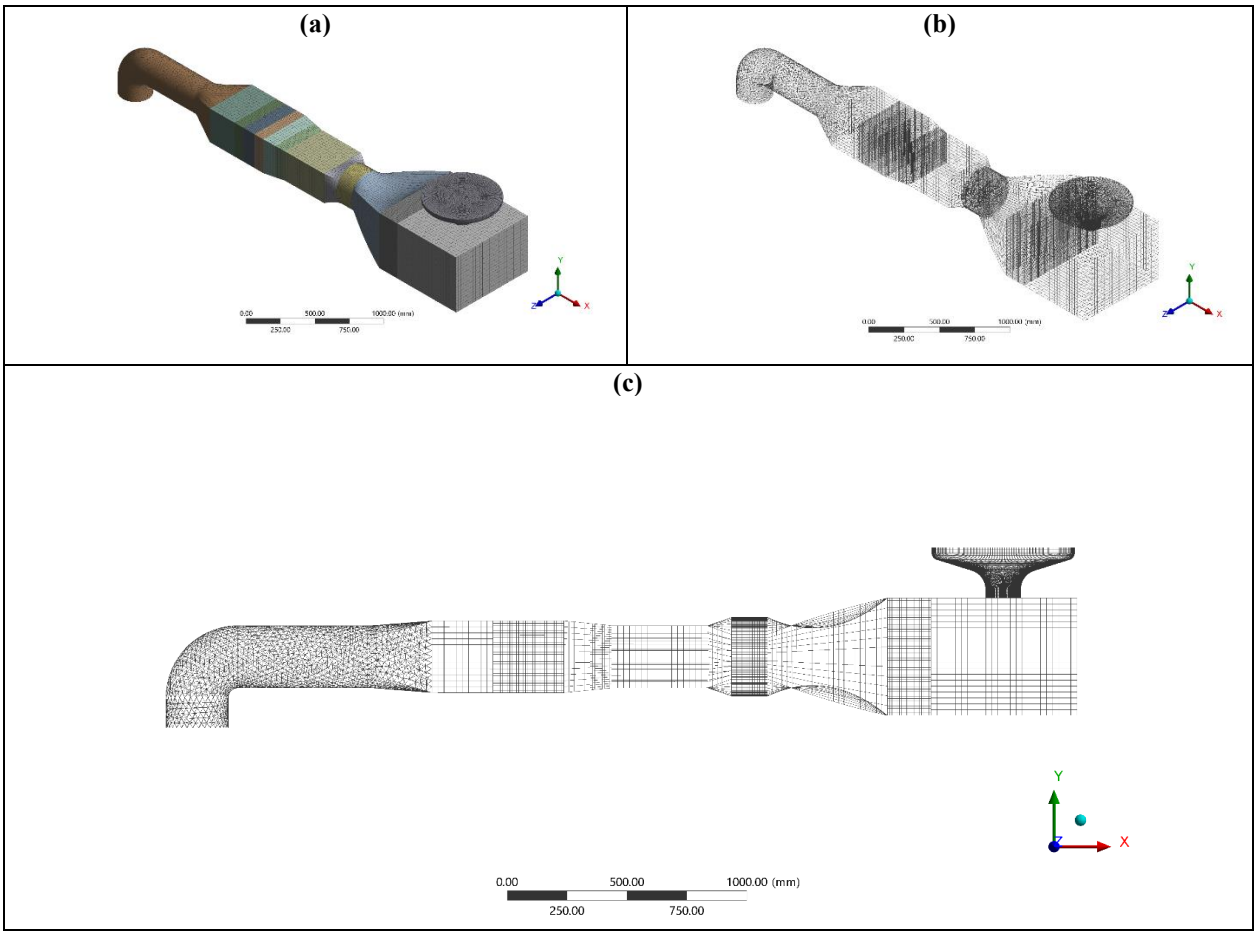


**Figure 3: Generated mesh (a) Mesh model, (b) Wireframe of the mesh, (c) End view of the filter system showing the meshed zones at the locations of the inlet air filters**

Conversely, the simulation did not consider variations in particle size distribution across the face area of individual filter elements; thus, pressure differential ($\Delta P_t$), and accumulated mass flow on each filter element ($\dot{m}_a$) was evaluated from Eq. (1) and (2) respectively. Filter loading efficiency, flow density, flow rate across each stage of the filtration, volumetric flow rate across the compressor, and sensible capacity, were also accounted for using Eq. (3) to (7) [26].

*Pressure differential ($\Delta P_t$):*

$$\Delta P_t = P_e - P_i \quad (1)$$

Where $P_e$ and $P_i$ are the filter exit and inlet pressures respectively.

*Accumulated mass flow on each filter element ($\dot{m}_a$):*

$$\dot{m}_a = \dot{m}_i - \sum(\dot{m}_A + \dot{m}_B + \dot{m}_C + \dot{m}_D + \dot{m}_E + \dot{m}_F) \quad (2)$$

Where $\dot{m}_i$ is the total inlet mass flow rate. $\dot{m}_A \ldots \dot{m}_F$ are the mass flow rates after the flow passes through the filters.

*Filter loading efficiency ($\eta_f$):*

$$\eta_f = \left(\frac{\dot{m}_e - \dot{m}_i}{\dot{m}_e}\right) \times 100 \quad (3)$$

Where $\dot{m}_e$ is the mass flow at the exit of filter, F.

*Flow density (ρ):*

$$\rho = \frac{P_s}{gh} \quad (4)$$

Where $P_s$, $g$, and $h$ are flow inlet static pressure, acceleration due to gravity, and flow head respectively.

*Flow rate across each stage of the filtration ($\dot{q}$):*

$$\dot{q} = \sqrt{\frac{2P_t}{\rho}} \quad (5)$$

Where $P_t$ is the total pressure, and $\rho$ is the air density.

*Volumetric flow rate across the compressor ($Q_f$):*

$$Q_f = \dot{q}\sqrt{\frac{\Delta P_s}{\Delta P_t}} \quad (6)$$

Where $\Delta P_s$ and $\Delta P_t$ are the static and total pressure differential across the compressor.

*Sensible capacity ($q_s$):*

$$q_s = Q_f \rho\left(c_p \Delta T\right) \quad (7)$$

Where $c_p$ is the specific heat capacity of air.

A solution was solved using the Naiver stokes equations, turbulence, and particle transport models presented in Eq. (8) to (10), to obtain the flow distribution characteristics [27, 28, 29]. The solution was executed in steady-state and transient conditions for time-independent and time-dependent analysis. Simulated contaminants (salt, aerosols, mist, dust, and particulate matter) each weighing 1000g were evaluated at mass loading between 20% to 100% on the filter elements [10, 30, 31]. The investigated flow characteristics include; inlet velocity (5 and 10m/s), static and total pressures, and mass flow at 298.14K and 1atm (101,325 Pa) [10, 26]. The solution was validated by comparing the results with the experimental results.

*Navier-Stokes equations:*

$$\frac{\partial \rho}{\partial t} + \nabla.(\rho u) = 0 \quad (8)$$

$$\frac{\partial (\rho u)}{\partial t} + \nabla.(\rho u u) = -\nabla p + \nabla.\tau + \rho g \quad (9)$$

Where $\rho$, $u$, $p$, $\tau$, and $g$ are the density of the fluid, velocity vector, pressure, viscous stress tensor, and gravitational acceleration respectively.

*The Continuity Equation describing the conservation of particles:*

$$\frac{\partial (\rho_p \emptyset_p)}{\partial t} + \nabla.\left(\rho_p u \emptyset_p\right) = \nabla.\left(\Gamma_p \nabla \emptyset_p\right) + S \quad (10)$$

Where $\rho_p$, $\emptyset_p$, $u$, $\Gamma_p$, and $S$ are the particle density, particle volume fraction, fluid velocity, particle diffusivity, and source terms respectively.

### *2.1 Grid refinement study*

The independence of the grid to the solution was assessed by carrying out a grid convergence study. This was done to avoid potential errors leading to an erroneous solution. The qualities of the grid were set to fine, medium, and coarse meshes. The mesh data is shown in Table 2.

**Table 2: Grid refinement study**

| Mesh Parameters | Fine | Medium | Coarse |
|---|---|---|---|
| Number of elements | 511210 | 340413 | 148181 |
| Number of nodes | 514794 | 339607 | 89487 |
| Aspect Ratio | 0.23 | 0.23 | 0.23 |
| Orthogonal Quality | 0.8 | 0.8 | 0.8 |
| Skewness | 0.3 | 0.3 | 0.3 |

## 3. RESULTS AND DISCUSSION

The simulation of the flow of contaminated particles into the GT inlet air filter apparatus conforms to the governing conditions for fluid flow through surfaces and porous media. This is evident in the CFD results presented. The solution was executed in steady-state and transient conditions for time-independent and time-dependent analyses. Figure 4 shows the end-view of velocity distribution across the filters. The air velocity is highest at the contraction in the inlet, with magnitudes approaching nine times the inlet velocity. This is because an increase in airflow velocity creates a corresponding pressure reduction.

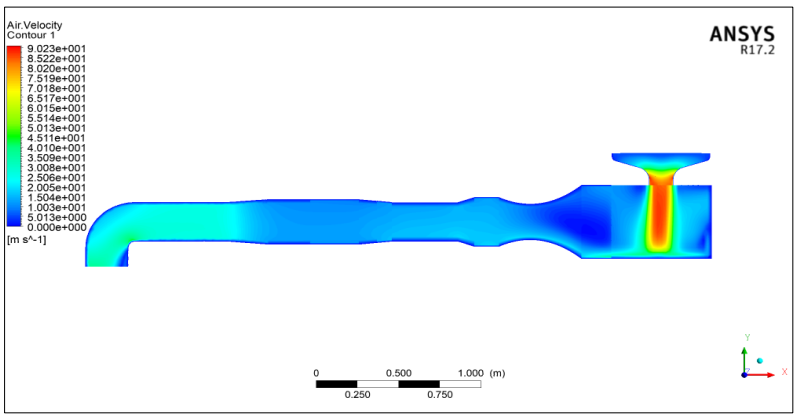


**Figure 4: Velocity contour of the GT air filter setup**

In the settling chamber, the airflow spreads with significant swirling, as seen in Figure 5. The flow of contaminated air subjected to the flow studies conforms with Bernoulli's principle.

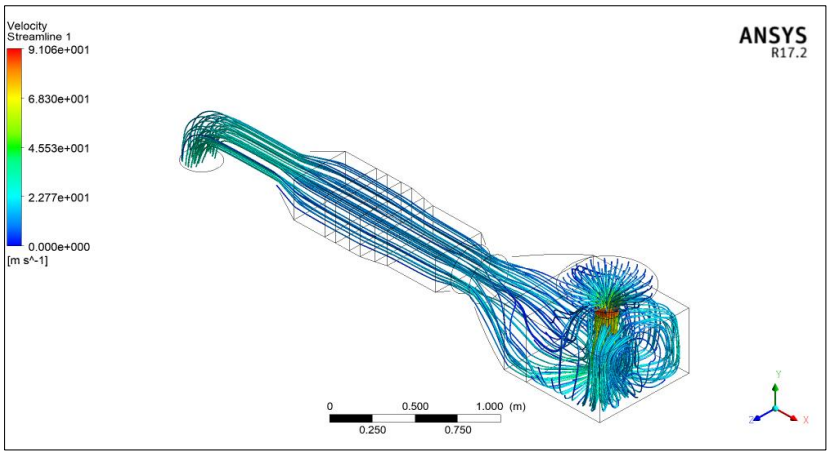


**Figure 5: 3-D visualization of the velocity streamlines across the filtration**

The visualization of velocity vectors was also examined during the post-processing. The result of the study is shown in Figure 6. In this case, the velocity vectors tend to concentrate at the location of the filters, marked also by a localized reduction in flow velocity. Also, by Bernoulli's principle, it can be seen that the intensity of the velocity vectors depends on the shape of the bounding chamber through which the flow is studied. Hence, at contractions, it is evident that the magnitudes of velocity increases. The flow is also very turbulent at the inlet settling chamber because the airflow direction into the filtration chamber is perpendicular to the flow across the air filters. The overall flow domain is also visualized in a three-dimensional velocity volume rendering, as shown in Figure 7.

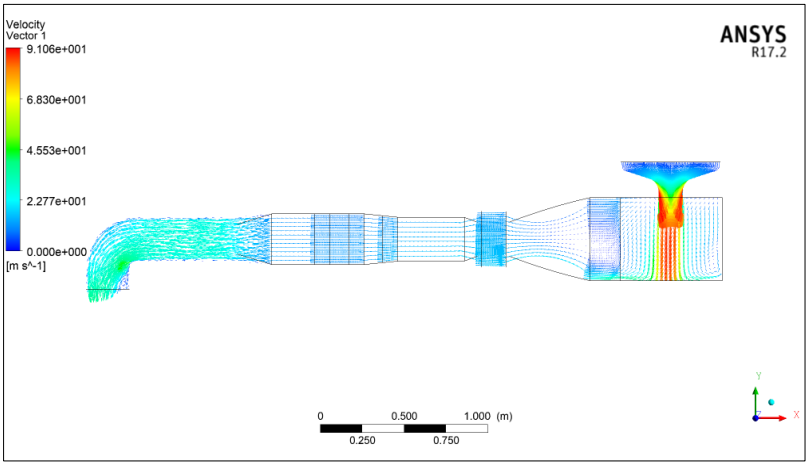


**Figure 6: End view of the filtration system showing the distribution of velocity vector**

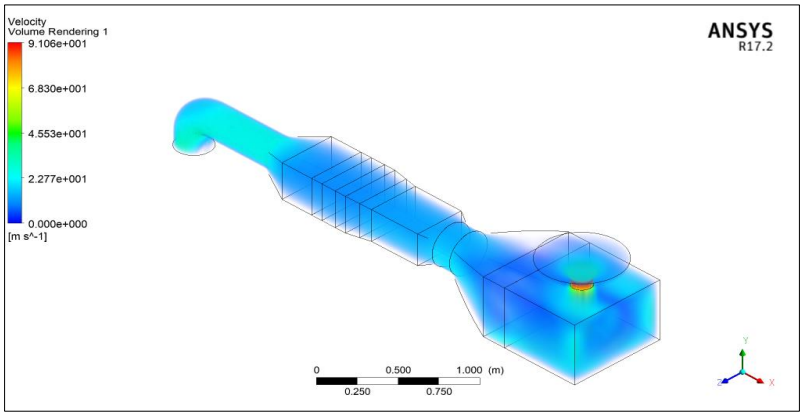


**Figure 7: Visualization of the velocity volume rendered in 3D**

Besides the flow velocity, mass flow distribution was also studied in the CFD post-processing stage. Figure 8 shows the contour of the mass flow distribution in the filtration system. It is evident that since inflow is directed vertically downwards and not parallel to the flow axis of the filter chamber, there is a marked concentration of mass flow directly opposite the inflow with magnitudes approaching 8.4 $kgs^{-1}$.

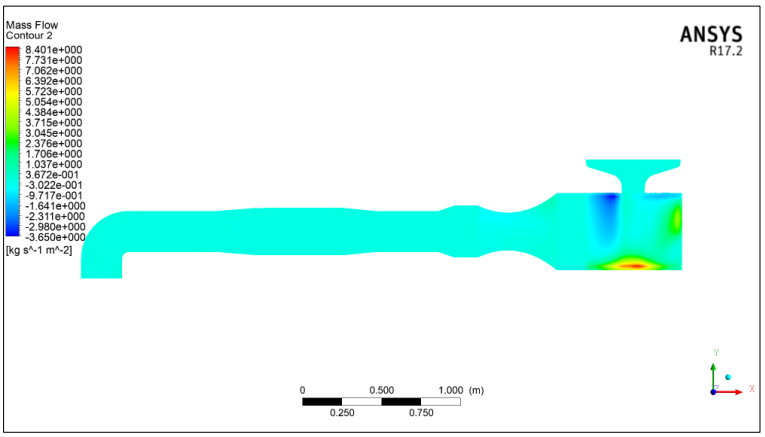


**Figure 8: Contour showing mass flow distribution in the equipment**

The static pressure distribution across the filter chamber is visualized in 2D, as shown in Figure 9. It is evident that the pressure is highest at the inlet and decreases as the air flows downstream. It can also be observed that the static pressure is also high at the region at the bottom of the setting chamber of the inlet domain directly opposite the inflow. In Figure 10, the static pressure distribution across the filter chamber is made more elaborate. Viewing the corners of the chamber, the static pressure is higher than the regions further from the walls of the test system.

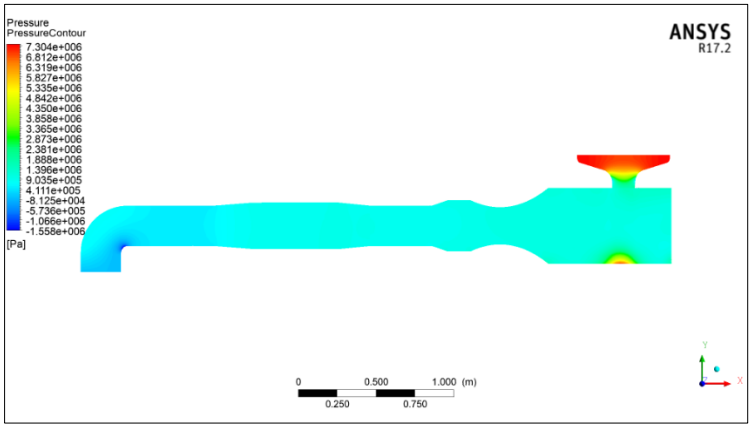


**Figure 9: 2D Visualization of the static pressure across the chamber**

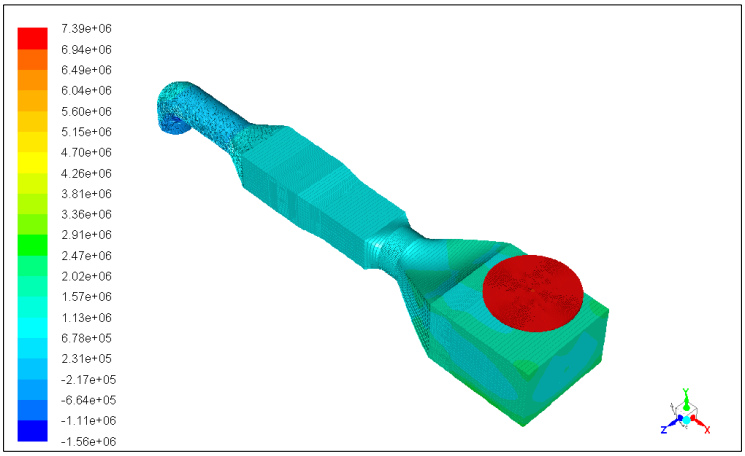


**Figure 10: Static Pressure distribution across the equipment shown in 3D**

Furthermore, the total pressure distribution was studied, as shown in Figure 11. The total pressure is observed to be higher at the inlet domain and decreases further downstream of the filtration system. There are also localized increase in magnitudes of the total pressure mostly at contraction zones and at corners in the chamber. The latter is because an increase in flow perpendicularly on the walls results in air being forced to the surfaces. Whereas in the free stream, the pressure due to the force of airflow on the walls of the chamber is lesser.

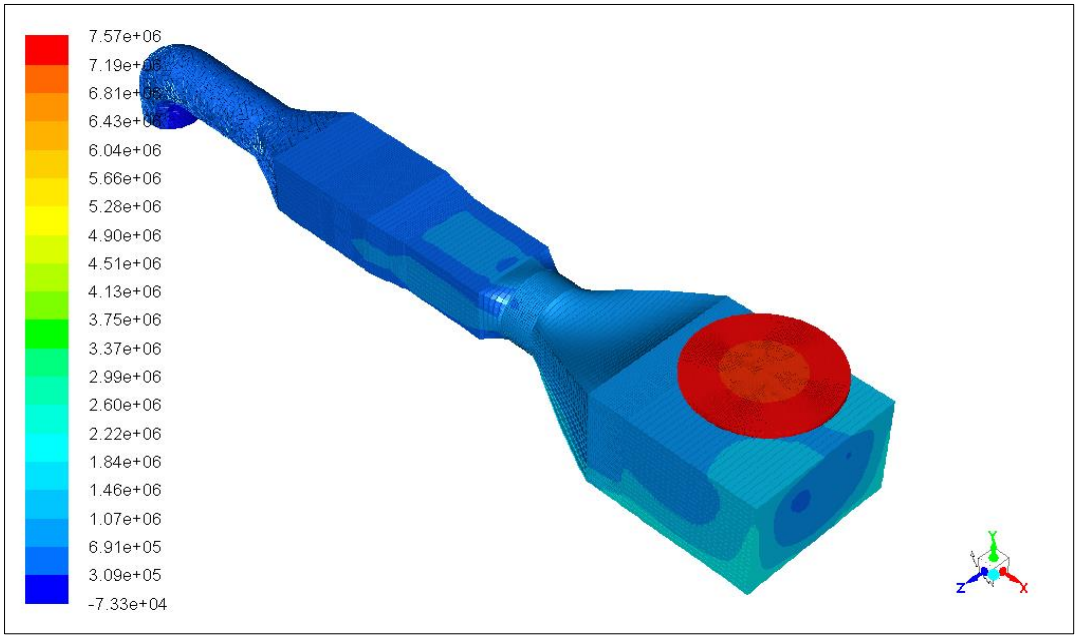


**Figure 11: 3D contours visualization showing the total pressure distribution**

### *3.1 Sensitivity analysis and results*

Studies were also carried out based on the data collected from the simulation to understand the relationships between mass loading, filtration efficiency, static pressure, total pressure, and time (for transient cases). The inlet velocities selected for these studies were 5 m/s and 10 m/s. Figure 12 shows the variation in static pressure with simulation time at velocities of 10 m/s and 5 m/s, respectively. The static pressure decreased with time based on the percentage of contaminants ingested. Longer operational times tend to have an adverse effect on the static pressure.

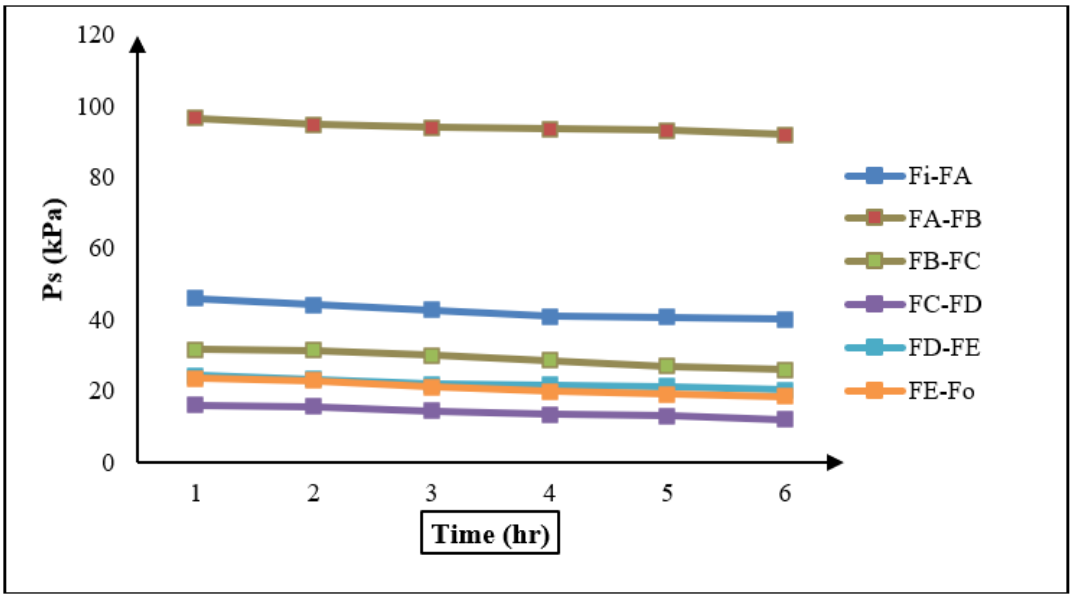


**Figure 12: (a) Static pressure variation with time at a velocity of 10 m/s**

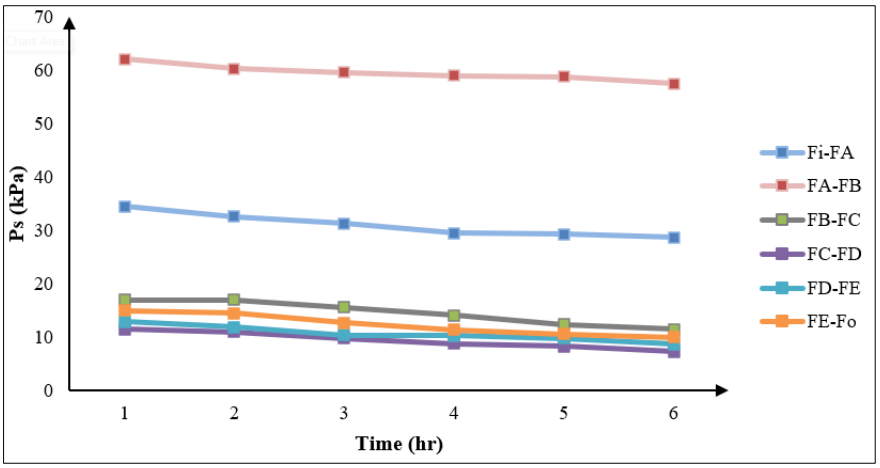


**Figure 12: (b) Static pressure variation with time at a velocity of 5m/s**

Also, the total pressure concerning the mass loading for the different filter elements was examined. The values for mass loading of ingested particles were increased from 20% to 100%. The results for the studies at 10 m/s and 5 m/s are presented in Figure 13. Considering the total pressure across the filters A to F, the percentage of ingested contaminants causes a decrease in the magnitude of the total pressure as it is increased from 20% to 100%. The reason for this is that as more contaminants are introduced to the flow stream, the resistance in the flow stream increases.

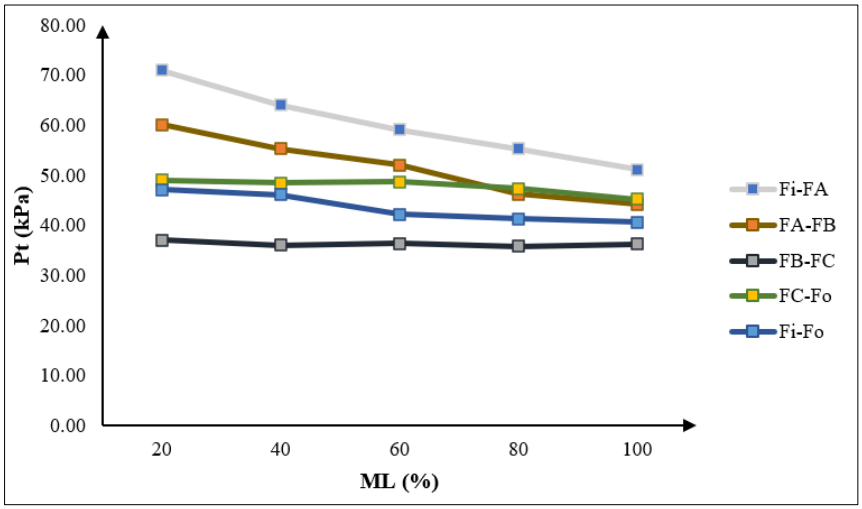


**Figure 13: (a) Total pressure variation with mass loading at velocity of 10 m/s**

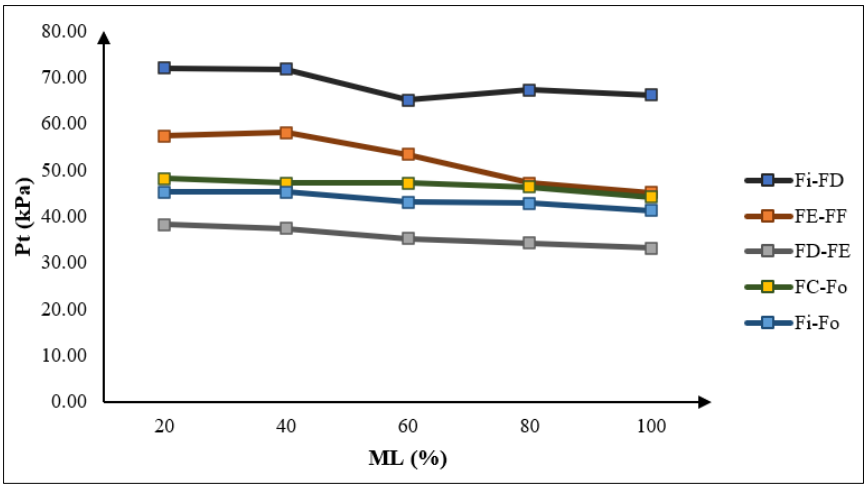


**Figure 13: (b) Total pressure variation with mass loading at velocity of 5 m/s**

Further studies were also carried out to assess the effect of mass loading on the pressure drop across the filter housing. The result of the study is shown in Figure 14 and indicates that the differential pressure is highest at filters FA – FB region. The magnitude of the differential pressure at this point is 6.34kPa. At that point, the inlet contaminant is at 80%. On the other hand, the lowest differential pressure occurs with the inlet contaminant (mass loading) of 20%, the corresponding differential pressure at this point was 1.22 kPa. This is be-cause as the quantity of contaminant increases, more resistance occurs at the inlet filter. Given also that the filter has a filtration efficiency of 90%, most of the injected contaminants are collected at that point. Furthermore, the filter pressure drop increases to a loading level of 90% to 100%. This occurs when the filter reaches a saturated state and can no longer capture more loaded contaminants. The pressure drop decreases at this point, but the overall filter efficiency when capturing particles decreases. Regularly monitoring pressure drop and timely filter cleaning or replacement is crucial to ensure optimal flow performance.

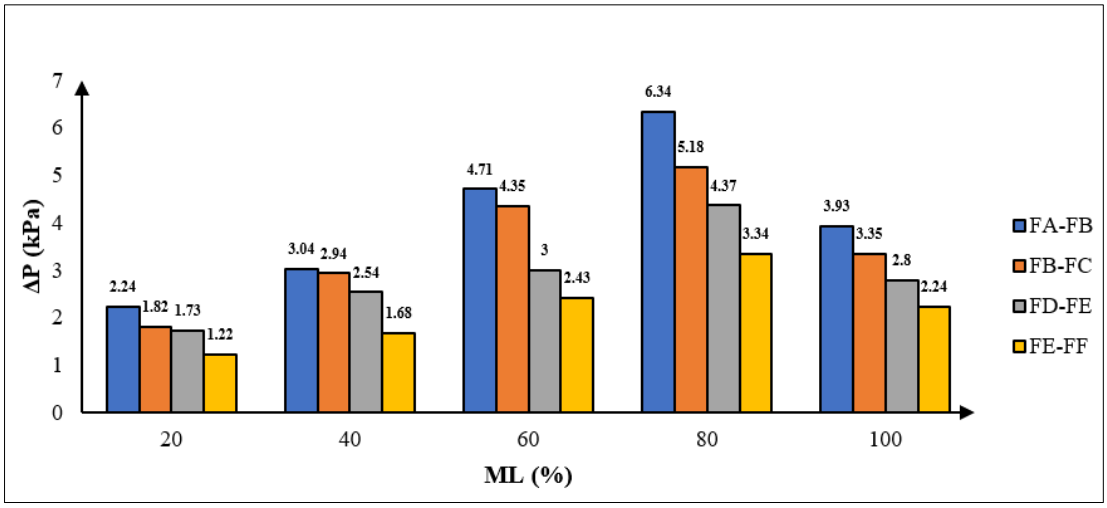


**Figure 14: Effect of mass loading on the pressure drop across the filter housing**

Also, Figure 15 shows the effect of time on filtration efficiency across the filter elements. The study was carried out in relation to time to determine the impact of the ingested particles on the filters. The filtration efficiency is also seen to decrease with time. The volume of ingested contaminants increases over time, leading to gradual decline in filtration efficiencies of the filters. This observation conforms with previous studies on a similar subject. In practice, such Fouling of the filters with time require periodic maintenance to ensure that the filtration system is still performing optimally.

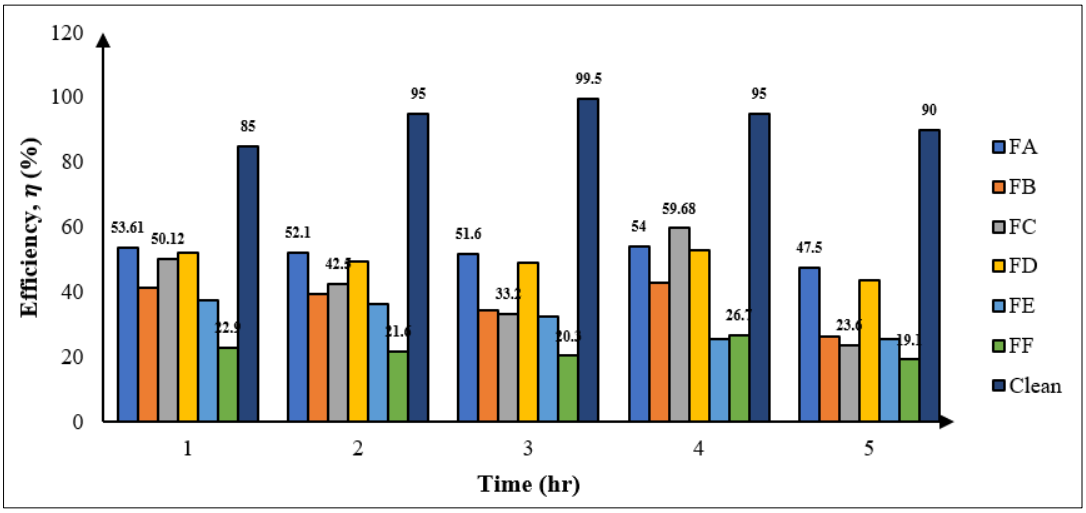


**Figure 15: Effects of filtration efficiency with time for different filter elements**

### 3.2 Result Validation

The result of the CFD study was validated by comparing the output of the CFD solution with the experimental study carried out by [10] using same modelling conditions. Table 3 compares the results of the differential total pressure and volumetric flow rates obtained from the CFD solution at 10 m/s and 5 m/s in relation to the experimental solutions.

**Table 3: Comparison of the CFD solution with the Experimental solutions**

| Outlet – Inlet | CFD | Experimental [10] | CFD | Experimental [10] |
|---|---|---|---|---|
| | 10 m/s | | 5 m/s | |
| $\Delta P_t$ (kPa) | 150.10 | 141.80 | 75.62 | 68.20 |
| $\Delta Q_f$ ($m^3/s$) | -1.10 | -1.03 | - 0.61 | - 0.57 |

The CFD results of differential total pressure ($\Delta P_t$) and volumetric flow rates ($\Delta Q_f$) as shown, indicate slight variation in comparison to the experimental values. At an inlet flow velocity of 10m/s, the % variation in $\Delta P_t$ and $\Delta Q_f$ is 5.52% and 6.36% respectively. Equally, at an inlet flow velocity of 5m/s, the % variation in $\Delta P_t$ and $\Delta Q_f$ is 9.81% and 6.56% respectively. This is evident in the results being relatively above the experimental by ≤10%. This could be due to the inherent complexities of the offshore environment, turbulent flows, and the various uncertainties involved in both simulation and experimental processes.

## 4 CONCLUSION

CFD model and analysis of a suitable multistage inlet filtration system for optimal offshore gas turbine application has been carried out at steady-state and transient conditions. The airflow dynamics, particle distribution, and pressure characteristics within the GT air filter apparatus was investigated. Validation against experimental data showed a slight variation with obtained CFD results by ≤10%. This could be due to the inherent complexities of the offshore environment, turbulent flows, and the various uncertainties involved in both simulation and experimental processes. The CFD results aligned with fluid flow principles and porous media conditions, evident in velocity, pressure, and mass flow patterns.

In summary, the CFD analysis provided comprehensive insights into the complex interactions within the GT air filtration system for offshore applications, aiding in understanding performance characteristics, transient effects, and the impact of contaminants on pressure and efficiency. This study is of great relevance to filter manufacturers and GT users for filter maintenance schedules and ensuring the long-term effectiveness of the filtration system.

**Nomenclature**

$\dot{m}$ – accumulated mass flow on each filter element, kg/s
$\dot{q}$ – Flow rate across the compressor, $m^3/s$
A – Filter class F7
B – Filter class H12
C – Filter class E11
D – Filter class E10
E– Filter class G5
F – Filter class F9
$h$ – flow head, m
P – Pressure differential, Pa
S – Particle size, $\mu m$
$P$ – pressure drop, Pa
$Q$ – Volumetric flow rate, $m^3/s$
$S$ – Source terms
$T$ – Temperature, K
$V$ – Nominal volume, $m^3/h$
$c$ – Specific heat capacity, kJ/kg.K
$g$ – acceleration due to gravity, $m/s^2$
$u$ – fluid velocity, m/s

**Greek symbols**

$\Delta$ – differential
$\eta$ – Loading efficiency, %
$\rho$ – air density, $kg/m^3$
$\emptyset$ - Volume fraction
$\Gamma$ – diffusivity, $m^2/s$
$\nabla$ – Divergence and special gradient
$\tau$ – Viscous stress tensor, Pa

**Subscripts and Superscripts**

1 – initial
2 – final
A – Filter class F7
B – Filter class H12
C – Filter class E11
D – Filter class E10
E – Filter class G5
F – Filter class F9
p – pressure
s – static
t – total
$e$ – exit
$f$ – filtration
$i$ – inlet
$p$ – Particle
$a$ – air

**Abbreviations and Acronyms**

ASHRAE – American Society of Heating, Refrigerating, and Air Conditioning Engineers
CAD – Computer Aided Design
CFD – Computational Fluid Dynamics
MPPS – Maximum power point speed, m/s

## REFERENCES

1. R. Banihabib and M. Assadi, “Towards a low-carbon future for offshore oil and gas industry: A smart integrated energy management system with floating wind turbines and gas turbines,” Journal of Cleaner Production, vol. 423, 138742, 2023.
2. I. A. Mohamed, I. A. Mustafa Kamal, K. Baharuddin, and S. S. Arudra, “Gas compressor driver selection for offshore application,” Offshore Technology Conference Asia, Kuala Lumpur, Malaysia, 2020, D012S001R054.

3. N. Dev, R. Kumar, R. K. Saha, A. Babbar, V. Simic, and N. Bacanin, "Performance evaluation methodology for gas turbine power plants using graph theory and combinatorics," International Journal of Hydrogen Energy, vol. 57, pp. 1286-1301, 2024.
4. G. H. Musa, "Techno-economic analysis of gas turbine compressor fouling and washing," Ph.D. dissertation, Dept. Mech. Eng., University Name, City, Country, 2019.
5. R. Kurz, K. Brun, and C. Meher-Homji, "Gas turbine degradation," Proceedings of the 43rd Turbomachinery Symposium, College Station, TX, USA, 2014, pp. 1-10.
6. J. Alqallaf and J. A. Teixeira, "Quantifying the economic benefits of using erosion protective coatings in a low-pressure compressor (aero-engine): A case study evaluation," Processes, vol. 10, no. 2, 385, 2022.
7. A. M. Al-Ibrahim and A. Varnham, "A review of inlet air-cooling technologies for enhancing the performance of combustion turbines in Saudi Arabia," Applied Thermal Engineering, vol. 30, pp. 1879-1888, 2010.
8. A. Suman, M. Morini, N. Aldi, N. Casari, M. Pinelli, and P. R. Spina, "A compressor fouling review based on an historical survey of ASME turbo expo papers," Journal of Turbomachinery, vol. 139, no. 4, 041005, 2017.
9. S. O. Effiom, F. I. Abam, and O. S. Ohunakin, "Performance modeling of industrial gas turbines with inlet air filtration system," Case Studies in Thermal Engineering, vol. 5, pp. 160-167, 2015.
10. S. O. Effiom, J. A. Ajor, P. C. O. Effiom, I. Edem, P. Ubi, F. Abam, and O. E. Diemuodeke, "Experimental study on the optimal performance of gas turbine (GT) inlet air filtration system for offshore application," Journal of Engineering and Applied Science, vol. 70, no. 1, 131, 2023.
11. M. G. De Giorgi, N. Menga, and A. Ficarella, "Exploring prognostic and diagnostic techniques for jet engine health monitoring: A review of degradation mechanisms and advanced prediction strategies," Energies, vol. 16, no. 6, 2711, 2023.
12. T. Dauxois, T. Peacock, P. Bauer, C. C. P. Caulfield, C. Cenedese, C. Gorlé, and A. W. Woods, "Confronting grand challenges in environmental fluid mechanics," Physical Review Fluids, vol. 6, no. 2, 020501, 2021.
13. S. Narayan and D. Bhalgat, "Geometry optimization of filter house components fitted at compressor entry," International Journal of Science and Research, vol. 3, pp. 905-909, 2014.
14. S. Howes, "Selecting gas-turbine inlet air systems for new retrofit applications," http://www.ccj-online.com/, (Accessed Jun. 10, 2024).
15. O. Brekke, L. E. Bakken, and E. Syverud, "Filtration of gas turbine intake air in offshore installation: The gap between test standard and actual operating condition," Proceedings of ASME Turbo Expo 2009: Power for Land, Sea, and Air, Orlando, FL, USA, 2009, pp. 1-2.
16. M. R. Chopade, A. P. Valavade, and S. H. Barhatte, "Performance evaluation of air filters by design optimization," International Journal of Advances in Engineering and Technology, vol. 3, no. 1, pp. 68-70, 2012.
17. S. Hosseinzadah, M. Gorji-Bandpy, G. J. Rad, and M. Keshavarz, "Experimental and numerical study of impact of air filter holes masking on altitude at heavy-duty diesel engine," Modern Mechanical Engineering, vol. 2, no. 4, pp. 157-166, 2012.
18. R. Manikantan and E. J. Gunasekaran, "Modelling and analyzing of air filter in air intake system in automobile engine," Advances in Mechanical Engineering, vol. 2013, 654396, 2013.
19. U. Igie and O. Minervino, "Impact of inlet filter pressure loss on single and two-spool gas turbine engines for different control modes," Journal of Engineering for Gas Turbines and Power, vol. 136, no. 9, 091201, 2014.
20. K. Khashayar, S. M. H. Karimian, M. Varmaziar, and S. Sarjami, "Investigation of flow pattern and pressure loss of a V94.2.5 gas turbine air intake system using 3D numerical modeling," http://www.wseas.us/e-library/conferences/2010/Cambridge/CFH/CFH-43.pdf, (Accessed Dec. 22, 2024).
21. U. Igie, D. Amoia, G. Michailidis, and O. Minervino, "Performance of inlet filtration system in relation to the uncaptured particles causing fouling in the gas turbine compressor," Journal of Engineering for Gas Turbines and Power, vol. 138, no. 1, 012601, 2016.
22. F. I. Abam, S. O. Effiom, and O. S. Ohunakin, "CFD evaluation of pressure drop across a 3D filter housing for industrial gas turbine plants," Frontiers in Energy, vol. 10, no. 2, pp. 192-202, 2016.
23. C. Vincenzo, L. Daniele, M. Marco, and G. Michele, "CFD simulation of filter houses for power plant gas turbine: Evaluation of differences between 2D and 3D models," http://dx.doi.org/10.6036/8913, (Accessed Jun. 10, 2021).
24. S. A. Abdul-Wahab, A. S. M. Omer, K. Yetilmezsoy, and M. Bahramian, "Modelling the clogging of gas turbine filter houses in heavy-duty power generation systems," Mathematical and Computer Modelling of Dynamical Systems, vol. 26, no. 2, pp. 119-143, 2020.
25. X. Tian, Q. Ou, Y. Lu, J. Liu, Y. Liang, D. Y. Pui, and H. Yi, "Influence of oil content on particle loading characteristics of a two-stage filtration system," Atmosphere, vol. 14, no. 3, 551, 2023.
26. M. Varmaziar and S. Sarjami, "Investigation of flow pattern and pressure loss of a V94.2.5 gas turbine air intake system using 3D numerical modelling," http://www.wseas.us/e-library/conferences/2010/Cambridge/CFH/CFH-43.pdf, (Accessed Jun. 10, 2024).

27. N. Gourdain, "Application of CFD to turbomachine-based systems," http://www.cerfacs.fr/~cfdbib/repository/TR_CFD_09_131.pdf, (Accessed Jun. 10, 2024).
28. ANSYS Inc., ANSYS ICEM CFD 19.0 User Manual, Canonsburg, PA, USA: SAS IP Inc., 2020, pp. 1-100.
29. T. H. Shih, W. W. Liou, A. Shabbir, Z. Yang, and J. Zhu, "A new κ-ε eddy viscosity model for high Reynolds number turbulent flows," Computers & Fluids, vol. 24, no. 3, pp. 227-238, 1995.
30. J. P. Stalder and J. Sire, "Salt percolation through gas turbine air filtration systems and its contribution to total contaminant level," Proceedings of the International Joint Power Generation Conference, New Orleans, LA, USA, 2001, pp. 445-456.
31. P. T. McGuigan, "Salt in the marine environment and the creation of a standard input for gas turbine air intake filtration systems," Proceedings of the ASME Turbo Expo: Power for Land, Sea, and Air, Vienna, Austria, 2004, GT2004-53113.